DSP-Based Current Control for Inverter-fed Permanent-Magnet Electrodynamic Shaker

Hung-Chi Chen (IEEE Member), Yu-Ching Lin and Jhen-Yu Liao
Department of Electrical Engineering, National Chiao Tung University, HsinChu, Taiwan.
hcchen@mail.nctu.edu.tw

***Abstract*- Compared to the conventional analog-circuit control and linear power amplifier for permanent-magnet electrodynamic shaker (PMEDS), a DSP-based digital current control with switched-mode power amplifier is proposed in this paper. A full-bridge converter is connected directly to PMEDS without LC filter in order to directly regulate the shaker current and simplify the digital current control. To meet the vibration requirement of wide operating range (typically 5~2kHz), the frequency of the unipolar switching scheme is increased to 50kHz PWM frequency in order to reduce the aliasing effect of the induced voltage and current harmonic sidebands. At the same time, dead-time compensation loop is also included in the digital current control to decrease the harmonics due to the dead-time in gate signals. The effectiveness of the proposed current control is verified by the provided simulation and measured results.**

I. INTRODUCTION

An electrodynamic shaker functions to deliver a force proportional to the current applied to its armature coil. These devices are used in such diverse activities as product evaluation, stress screening, squeak-and-rattle testing and modal analysis. These shakers may be driven by sinusoidal, random or transient signals based upon the application. In order to meet the stringent requirement of low armature current distortion over a wide frequency range (typically, 5-2kHz), the electrodynamic shaker is invariably driven by an audio-frequency power amplifier. It is conventionally powered by AC linear power supply with controlled voltage and controlled frequency [1-3]. However, it possesses the disadvantages of large size, large weight and low efficiency.

During the last decades, more and more attentions are put on the power electronics and control techniques to reduce the output harmonics. Compared to linear power supply, the switching-mode power supply has the advantages of small size, small weight and high efficiency [4]. Therefore, some inverter-fed electrodynamic shaker control had been proposed in [5-8] and all are implemented with analog circuits.

In addition, the full-bridge converter is connected directly to the electrodynamic shaker in [5]. It follows that the output current of the full-bridge converter is identical to the shaker current (i.e. armature current), and the current harmonics resulting from the output voltage harmonic would flow through the shaker armature.

In order to avoid the unexpected vibration harmonics due to the current harmonics, some LC filters are connected between the full-bridge converters and the electrodynamic shakers to reduce the current harmonics in [6-8]. On the other hand, the controllable converter current is not identical to the desired shaker current for those topology with LC filter, which would introduce some complexity to the current controller design. Similar conditions with cascading LC filter can also be found in [9-11].

In order to overcome such "indirect control" problem, many control techniques had be proposed and implemented, such as command feedforward control [6-7], disturbance feedforward control [6-7], second-order predictive control [9], and method of controlled-capacitor-charging [10-11]. All solutions are complicated and need sensing capacitor voltage.

Due to the line frequency (50Hz or 60Hz) in the applications [9-11], the complicated controls are able to be digitally implemented. Unfortunately, for the maximum operating frequency (2kHz) of electrodynamic shaker, it is hard to digitally implement the complicated controls because of the high digital sampling frequency and thus, the proposed controls in [6-8] are implemented with analog circuits.

In order to avoid the complicated control resulting from LC filter, in this paper, a full-bridge converter is connected directly to the electrodynamic shaker and a relatively simple control with only feedback loop and dead-time compensation loop is proposed and digitally implemented in DSP-based system. The simulation results and experimental results also demonstrate the proposed control.

The paper is organized as follows. In first, the mechanism and governed equations of a permanent-magnet electrodynamic shaker (PMEDS) are studied. At the same time, the behavior of a full-bridge converter with unipolar switching scheme and the resulting dead-time effect are also represented as several block diagrams. Then, the proposed current control is designed and implementd. Finally, some simulated and experimental results have been given to demonstrate the performance of the proposed current control for PMEDS.

II. PERMANENT-MAGNET ELECTRODYNAMIC SHAKER

The cut-view plot of PMEDS is show in Fig. 1 where the permanent-magnet yields a constant and homogeneous flux density B at the air gap between the armature coil and iron core. The flowing direction of armature current i_a and the direction of air-gap flux density are perpendicular to one another. Thus, the generated force f_e upon each conductor at the magnetic field is

$$f_e = NB\ell i_a = \Gamma i_a \tag{1}$$

where ℓ is the effective length of each conductor and N is the effective number of conductor in the magnetic field.

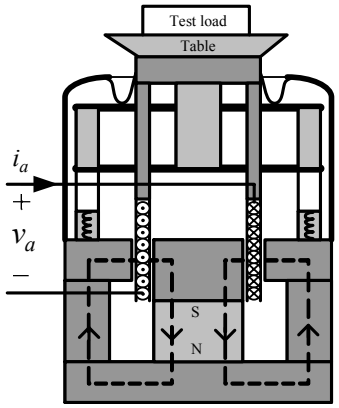

Fig. 1. Permanent-magnet electrodynamic shaker (PMEDS).

A. Mechanical Governed Equation

Under the assumptions that the test load is free of resonances and rigidly attached to the table, the shake table moves very much like the one-degree-of-freedom (1DOF) system as shown in Fig. 2 and the mechanical governed equation can be easily expressed as

$$f_e = m\frac{d^2x}{dt^2} + c\frac{dx}{dt} + kx \tag{2}$$

where x is displacement of the movement of the shaker from standstill and m is the total mass of the movement plus the test load. k and c are the shaker suspension stiffness and damping coefficient, respectively.

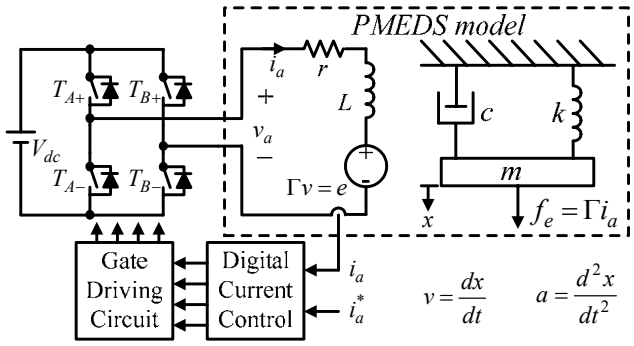

Fig. 2. System configuration and PMEDS model.

B. Electrical Governed Equation

The conductor moving within the magnetic field would induce some voltage across each conductor and the lumped induced voltage (i.e. back electromotive force, back-EMF) e across the armature can be expressed

$$e = \Gamma v = \Gamma\frac{dx}{dt} \tag{3}$$

Then, the corresponding differential equation relating the armature voltage v_a to the armature current i_a is obtained from Fig. 2

$$v_a = ri_a + L\frac{di_a}{dt} + e \tag{4}$$

C. PMEDS parameters

Since the used PMEDS V406 in this paper is the same as the one in [5], the estimation technique developed in [5] is applied as an alternative to find the parameters. The results are

$$\begin{aligned} &m = 0.245kg, \quad k = 13143N/m, \\ &c = 3.54N\cdot s/m, \quad \Gamma = 12.3N/A \end{aligned} \tag{5}$$

The estimated armature resistance and inductance at frequency $2kHz$ are

$$r = 2.9\Omega, \quad L = 0.1mH \tag{6}$$

III. Full-Bridge Converter

A. Unipolar Switching Scheme

As shown in Fig. 2, the full-bridge topology is used to obtain the controllable armature voltage v_a. Generally speaking, three PWM schemes, bipolar switching scheme, unipolar switching scheme and voltage cancellation scheme may be used to generate the four gate signals for full-bridge topology.

For the application of electrodynamic shaker, the sinusoidal armature current is necessary and thus, the voltage harmonics should be reduced as soon as possible. Therefore, the unipolar switching scheme is used in this paper and the single-carrier and multi-carrier schemes are plotted in Fig. 3(a) and Fig. 3(b), respectively, where the triangular carrier v_{tri} (not sawtooth signal) is used and the triangular carrier v_{tri2} is phase shifted by 180° from the other carrier v_{tri1}.

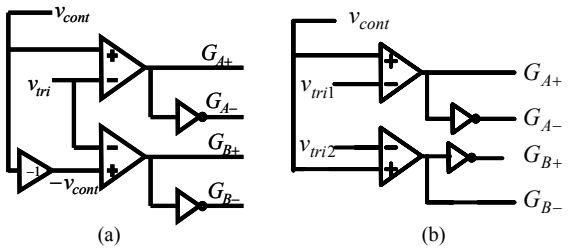

(a) (b)

Fig. 3. (a) Single-carrier unipolar switching scheme; (b) multi-carrier unipolar switching scheme.

In fact, adequate dead-time between the gate signals is necessary to avoid short-circuit condition. However, the design of dead-time mechanism would result in voltage saturation.

B. Effect of Dead Time

In order to understand the effect of dead time on the output voltage, the gate signals and the resulting output voltage without dead time and with dead time t_Δ are plotted in Fig. 4(a) and Fig. 4(b), respectively.

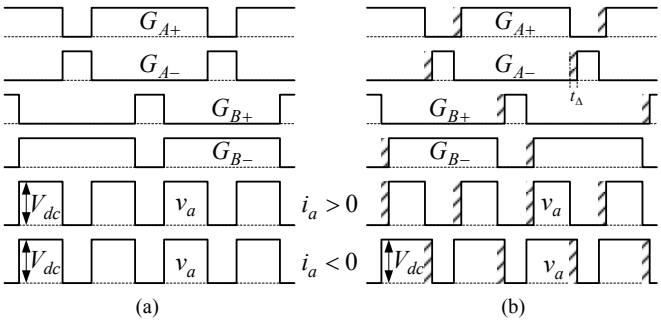

Fig. 4. Gate signals and the resulting armature voltage v_a : (a) without dead time t_Δ ; (b) with dead time t_Δ .

When the armature current i_a is positive, the resulting average voltage $\bar{v}_a$ in Fig. 4(b) is smaller than the ideal average voltage $\bar{v}_a$ in Fig. 4(a) with $V_{dc} f_{PWM} t_\Delta$ where f_{PWM} is the PWM frequency and carrier frequency. Contrarily, the resulting average voltage $\bar{v}_a$ in Fig. 4(b) is larger than the ideal average voltage $\bar{v}_a$ in Fig. 4(a) with the identical amplitude $V_{dc} f_{PWM} t_\Delta$ due to the negative armature current. Therefore, the dead-time effect on output voltage can be represented as

$$\Delta\bar{v}_a = -2sign(i_a) V_{dc} f_{PWM} t_\Delta \tag{7}$$

where $sign(x)$ is a sign function.

With the carrier signal varying between +1 and -1 in Fig. 3, the average armature voltage can be represented as

$$\bar{v}_a = v_{cont} V_{dc} - \Delta\bar{v}_a \tag{8}$$

Generally speaking, the dead time t_Δ is selected according to the turning-on time and turning-off time on the datasheet of the used power switch. However, the maximum operating frequency of PMEDS is high to $2kHz$ and the used PWM frequency should be high enough to yield the closed current tracking performance. It means that the dead-time effect of PMEDS application is much larger than that of other applications, such as motor driving. Thus, a dead-time compensation is included in the following digital current control to alleviate the dead-time effect.

IV. Proposed Current Control

The derived transfer function of PMEDS from (1)-(4) and the modeling of full-bridge converter from (7)-(8) are plotted in Fig. 5. By neglecting the dead-time term $\Delta\bar{v}_a$ in Fig. 5, the transfer function of plant including PMEDS and full-bridge converter is

$$\frac{i_a(s)}{v_{cont}(s)} = \frac{V_{dc}\dfrac{1}{sL+r}}{\dfrac{1}{sL+r}\dfrac{\Gamma^2 s}{ms^2+cs+k}+1} \tag{9}$$

In order to yield the closed current tracking performance, the proposed current control includes a proportional-plus-integral (PI) feedback loop, a command feedforward loop and a dead-time compensation loop, i.e.

$$v_{cont} = v_b + v_f + v_c \tag{10}$$

where v_b is the output of the feedback loop and $v_c = 2sign(i_a) f_{PWM} t_\Delta$ is the compensation term.

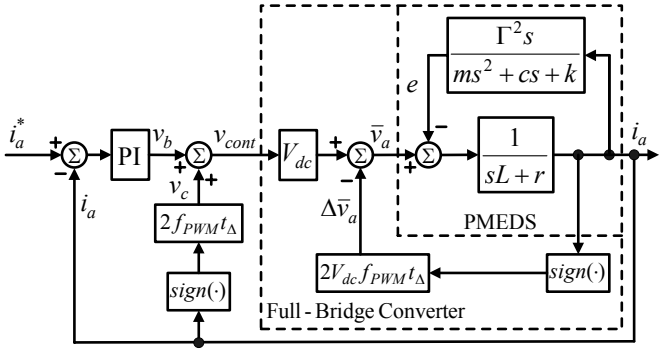

Fig. 5. Proposed current control for PMEDS.

Since the compensation term v_c in the proposed controller is able to cancel the dead-time voltage $\Delta\bar{v}_a$ in the full-bridge converter, the closed-loop transfer function of the overall current loop is

$$\frac{i_a(s)}{i_a^*(s)} = 1 \tag{11}$$

If all the parameters in Fig. 5 are identical the actual parameters in Fig. 2, the feedback loop in the proposed current control could be removed. However, parameter mismatch exists in the practical system, and thus the feedback loop is not only to regulate the armature current, but to reduce the effect of parameter mismatch on the armature current.

The used parameters of full-bridge converter are as follows:

$$V_{dc} = 80V, \quad f_{PWM} = 50kHz, \quad t_\Delta = 0.5\mu s \tag{12}$$

V. Simulation Results

By using the parameters in (5), (6) and (12), some simulation results of ideal current source and the proposed current control are provided in this section.

A. Fed by Ideal AC Current Sources

In order to understand PMEDS characteristics, the simulation results of a PMEDS fed by ideal AC current sources 10Hz/1A, 30Hz/1A, 2kHz/1A are plotted in Fig. 6(a), Fig. 6(b), and Fig. 6(c), respectively, and its equivalent block diagram is shown in Fig. 7. Thus, the armature voltage v_a is the sum of the induced back-EMF e and the voltage drop v_z across the armature winding.

When the frequency of current source to PMEDS is low in Fig. 6(a), both induced back-EMF e and the voltage drop v_z are small. As the source frequency increases to closed to the resonant frequency, the armature voltage is dominated by the rapidly increasing induced back-EMF e.

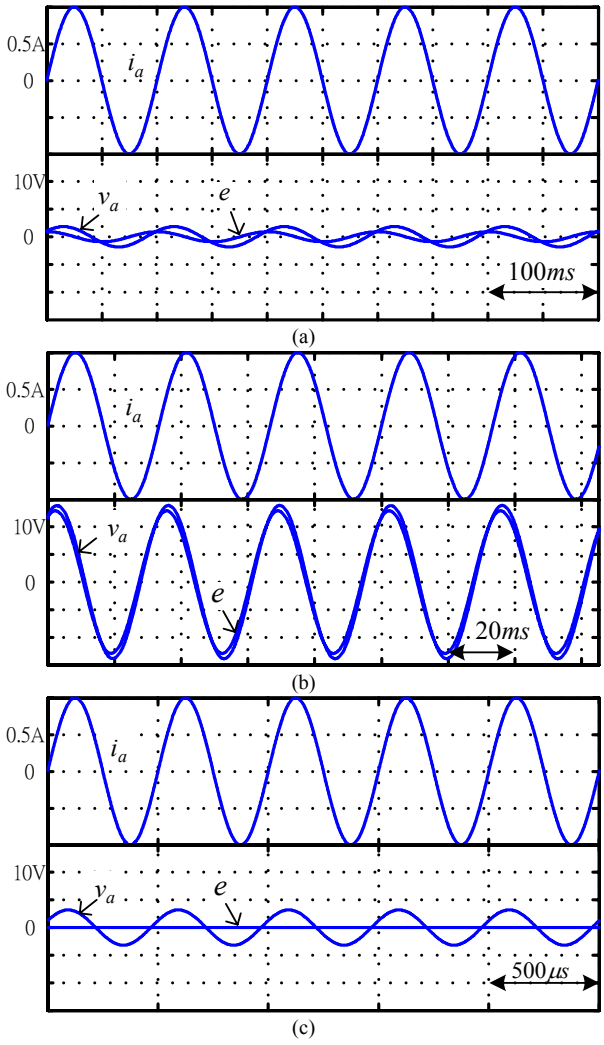

Fig. 6. Simulation results of PMEDS fed by ideal current source: (a) 10Hz/1A; (b) 30Hz/1A; (c) 2kHz/1A.

When the current source frequency increases far from the resonant frequency, the induced back-EMF e decreases rapidly, but the voltage drop v_z across the armature winding still increases. Thus, the voltage v_z is gradually dominant in the armature voltage.

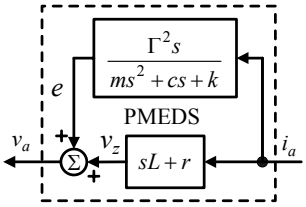

Fig. 7. Equivalent block diagram for PMEDS

B. Fed by Proposed Current Control

The simulation results by proposed current control without feedforward loop and dead-time compensation loop are plotted in Fig. 8.

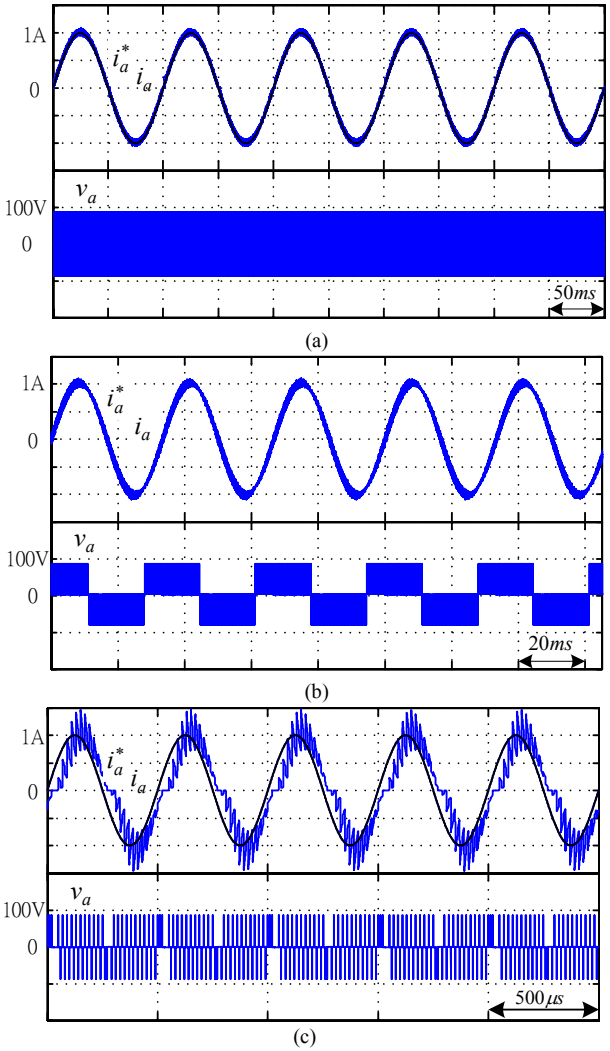

Fig. 8. Simulation results of PMEDS fed by full-bridge circuit : (a)10Hz/1A; (b)30Hz/1A; (c)2kHz/1A.

Since the induced back-EMF is relatively small at small frequency, the feedback loop is able to yield the closed current tracking performance in Fig. 8(a), and the significant dead-time effect on the armature voltage can be found due to the small control signal.

In the case of near resonant frequency ($\approx 36Hz$) as shown in Fig. 8(b), in order to overcome the induced back-EMF, the control signal becomes large to provide adequate armature voltage and the armature voltage is similar to the common unipolar waveform. However, the current tracking performance is also accepted in Fig. 8(b).

When the frequency is increased to 2kHz as plotted in Fig. 8(c), the induced back-EMF is smaller than the case in Fig. 8(b), but the feedback loop loses the closed current tracking performance due to the dead-time effect.

Then, the simulation result with only feedback loop and dead-time compensation loop is plotted in Fig. 9 where a closed current tracking performance is found.

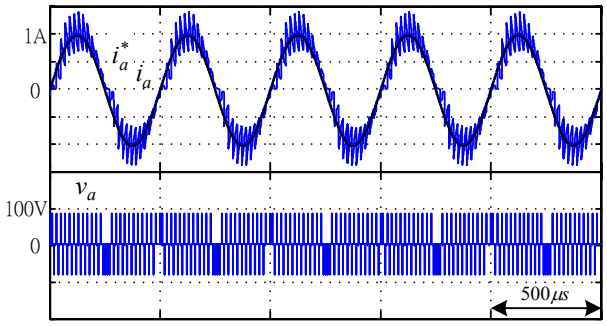

Fig. 9. Simulation results of PMEDS fed by full-bridge circuit with dead-time compensation loop at 2kHz/1A.

VI. Experimental Results

The proposed current control has been digitally implemented in a DSP-based system using TMS320F2812 and all the experimental parameters had been listed in (5), (6) and (13). Both the sampling frequency of control loop and A/D conversion are 50kHz to keep with the PWM frequency. A accelerometer is mounted in the PMEDS table to monitor the acceleration signal a.

The experimental results with only feedback loop for armature current command 10Hz/1A, 30Hz/1A, 40Hz/1A, 1kHz/1A and 2kHz/1A are plotted in Fig. 10(a), Fig. 10(b), Fig. 10(c), Fig. 10(d) and Fig. 10(e), respectively.

Fig. 10(a), Fig. 10(b) and Fig. 10(c) show closed current tracking performance of the proposed current control at small frequency, but the experimental system gradually loses the closed current tracking performance with high frequency as shown in Fig. 10(d) and Fig. 10(e). The maximum acceleration rate measured by accelerometer is about $200\,m/s^2$ ($\approx 20g$) as shown in Fig. 10(b) and Fig. 10(c) when the frequency is closed to the resonant frequency

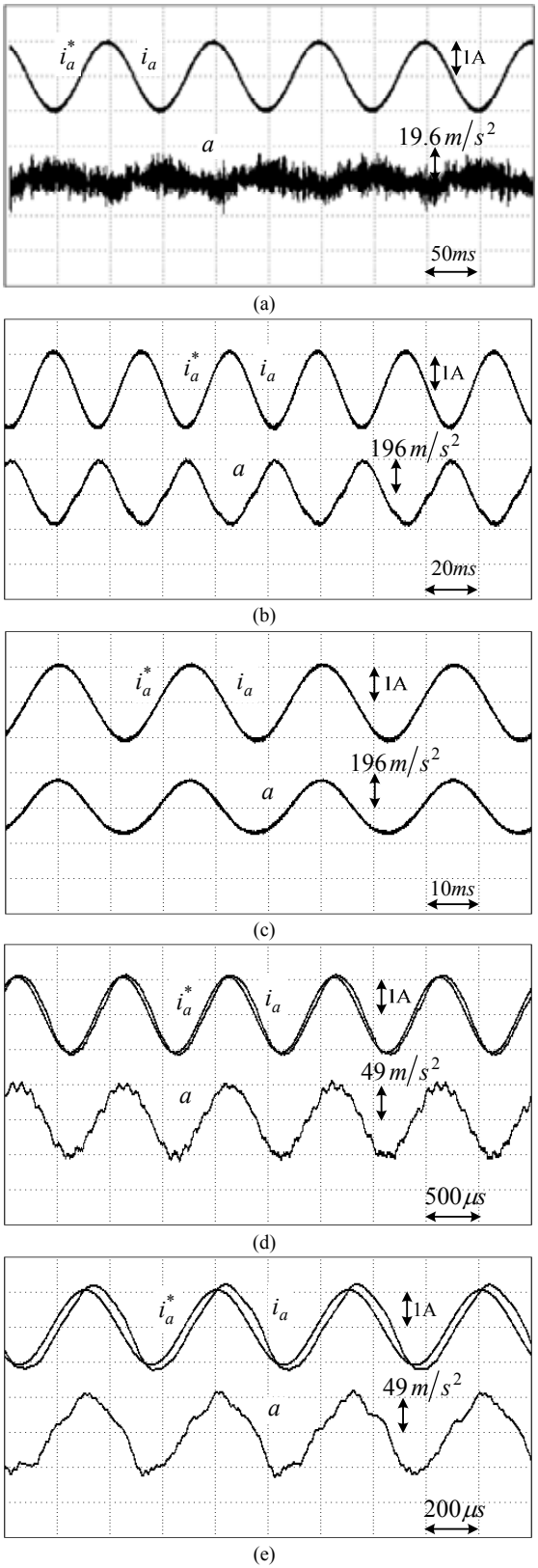

Fig. 10. Experimental results with only feedback loop: (a) 10Hz/1A; (b) 30Hz/1A; (c) 40Hz/1A; (d) 1kHz/1A; (e) 2kHz/1A.

Then, the experimental results with only feedback loop and dead-time compensation loop at current command 1kHz/1A and 2kHz/1A are plotted in Fig. 11(a) and Fig. 11(b), respectively. Compared to Fig. 10(e) and Fig. 10(f), the closed current tracking performance is obtained by including the dead-time loop and thus, the distortions in the acceleration signal a are also reduced.

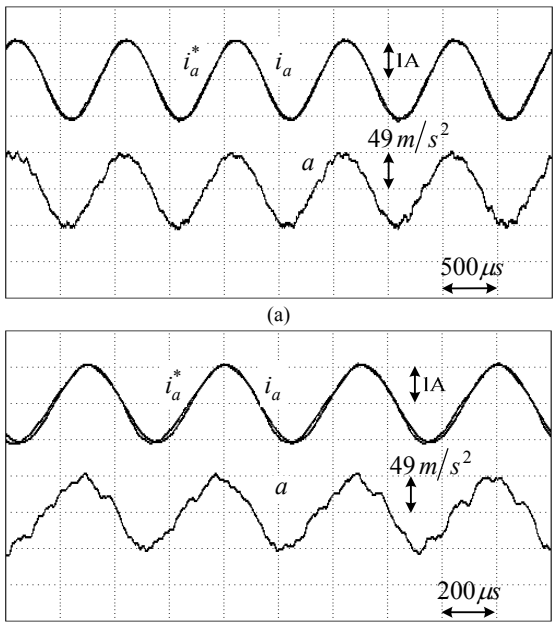

Fig. 11. Experimental results with only feedback loop and dead-time compensation loop: (a) 1kHz/1A; (b) 2kHz/1A.

In order to evaluate the performance of sweeping current command frequency, the experimental result of increasing current command frequency is plotted in Fig. 12. The yielded armature current i_a is closed to the current command i_a^* and the measured maximum acceleration rate is high to $490\,m/s^2$ $(\approx 49g)$.

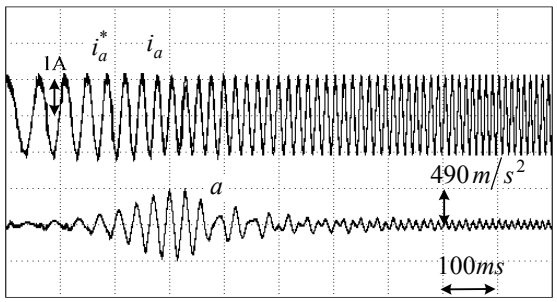

Fig. 12. Experimental result with sweeping frequency *f*.

VII. CONCLUSIONS

Modeling of PMEDS and full-bridge converter has been finished and the DSP-based current control has been designed and implemented in this paper. The current tracking performance is improved by the proposed dead-time compensation loop. The sinusoidal and random acceleration control are the future work.

REFERENCES

[1] L. D. Flora and H. A. Grudling, "Acceleration Control of an Inverter-fed Electrodynamic Shaker," in *Proc. IEEE Power Electronics Specialists Conference* (*PESC*), pp. 2799–2805, Jeju, Korea, June 2006.

[2?] Y. Uchiyama and M. Fujita "Robust Acceleration and Displacement Control of Electrodynamic Shaker," *IEEE International Conference on Control Applications* (*CCA*), pp. 746-751, 2006.

[3] L. D. Flora and H. A. Grudling, "Time Domain Sinusoidal Acceleration Controller for an Electrodynamic Shaker," *IET Control Theory Appl*., vol. 2, no. 12, pp. 1044–1053, Dec. 2008.

[4] N. Mohan, T. M. Undeland, and W. P. Robbins, *Power Electronics: Converter, Applications and Design,* 2nd ed. New York: Wiley, 1995.

[5] T. H. Chen, K. C. Huang and C. M. Liaw, "High-Frequency Switching-Mode Power Amplifier for Shaker Armature Excitation," *IEE Proc.-Electr. Power Appl.,* vol. 144, no. 6, Nov. 1997.

[6] T. H. Chen and C. M. Liaw, "Vibration Acceleration Control of an Inverter-Fed Electrodynamic Shaker," *IEEE/ASME Trans. on Mechatronics*, vol. 4, no. 1, March 1999.

[7] C. M. Liaw, W. C. Yu and T. H. Chen "Random Vibration Test Control of Inverter-Fed Electrodynamic Shaker," *IEEE Trans. on Industrial Electronics*, vol. 49, no. 3, June 2002.

[8] J. Han, T. Tang, and X. Wang, "A High-Performance Switching Mode Power Amplifier for Electrodynamic Shaker," *IEEE The Department of Electrical Engineering Shanghai Maritime University*, pp.491-495 2005.

[9] E. Oyarbide, J. Galarza, S. Aurtenechea and M. A. Rodriguez, "Second-Order Predictive Direct Control of a Voltage Source Inverter Coupled to an LC Filter," *IET Power Electron.,* vol. 1, no. 1, pp. 38-49, 2008.

[10] S. Dalapati and C. Chakraborty, 'A Direct PWM Technique for a Sungle-Phase Full-Bridge Inverter Through Controlled Capacitor Charging,' *IEEE Trans. on Industrial Electronics*, vol. 55, no. 8, Aug. 2008.

[11] S. Dalapati and C. Chakraborty, 'Performance Evaluation of Controlled-Capacitor-Charging-Type Inverter,' *IEEE Trans. on Industrial Electronics*, vol. 56, no. 1, Jan. 2009.